PERGAMON Computers and Mathematics with Applications 43 (2002) 927–941

An International Journal
computers & mathematics
with applications

www.elsevier.com/locate/camwa

An Inversion Method for Parabolic Equations Based on Quasireversibility

M. TADI
Department of Mechanical Engineering, University of Colorado at Denver
Campus Box 112, P.O. Box 173364
Denver, CO 80217-3364, U.S.A.

M. V. KLIBANOV AND WEI CAI
Department of Mathematics. University of North Carolina at Charlotte
Charlotte, NC 28223, U.S.A.

(Received January 2001; revised and accepted June 2001)

Abstract—This paper is concerned with a new method to solve a linearized inverse problem for one-dimensional parabolic equations. The inverse problem seeks to recover the subsurface absorption coefficient function based on the measurements obtained at the boundary. The method considers a temporal interval during which time dependent measurements are provided. It linearizes the working equation around the system response for a background medium. It is then possible to relate the inverse problem of interest to an *ill-posed* boundary value problem for a differential-integral equation, whose solution is obtained by the method of quasireversibility. This approach leads to an iterative method. A number of numerical results are presented which indicate that a close estimate of the unknown function can be obtained based on the boundary measurements only. © 2002 Elsevier Science Ltd. All rights reserved.

Keywords—Parabolic equations, Inversion, Quasireversibity.

1. INTRODUCTION

In this paper, a second generation of the so-called 'elliptic systems method' (ESM) [1,2] for the numerical solution of parabolic inverse problems is developed. The first generation of the ESM only allowed one to image locations of the unknown small size targets, while the unknown coefficients within those targets were imaged poorly, with their values being at least ten times less than the correct ones [1]. It is shown in this paper, however, that the second generation method enables one to image with good accuracy both the locations of targets, and the values of unknown coefficients within them. In this approach, the difference between maximal values of computed coefficients within targets and their correct values usually does not exceed 25%.

Inverse problems for parabolic equations appear in various fields with different applications. For instance, in electronic devices, the vital metal parts are routinely tested for coating quality or hidden corrosion or adhesion problems [3]. In thermal systems, various thermal properties, including heat convection coefficient [4] and temperature dependent thermal conductivity [5] are often unknown and need to be recovered. Recent applications also include the optical imaging

The work of all three authors was supported by grants from the National Science Foundation. They are CCR-9972251 for Tadi and Cai and DMS-9704923 for Klibanov.

0898-1221/02/$ - see front matter Typeset by AMS-TEX
PII: S0898-1221(01)00335-2

where the interest is to recover abnormal anomalies in human tissues [6,7]. In most applications, one is led to excite the system by an external means and record the associated system response. The collected data is then used to recover the sought-after unknown. For example, in applications involving nondestructive evaluation (NDE), also known as thermal imaging, one makes use of laser sources to illuminate an external surface of the material in order to induce thermal waves. The interactions of the thermal wave field with the material inhomogeneities give rise to the scattered fields which propagate and are ultimately measured at the surface of the material.

Motivated by numerous physical applications, inverse problems for parabolic equations have received considerable attention. Recent results include an analytical method for the solution of the overdetermined inverse heat conduction [8], application of neural networks for the recovering of electrical conductivity profile [9], a spectral method for solving the sideway heat equations [10], and a discrete diffusive model for the recovery of the absorption coefficient from diffused reflected light [11]. Also, additional methods for various applications include nonlinear optimization using genetic algorithms [12], Marquardt's procedure [13], and thermal wave slice tomography [14]. Recent analytical results have also been reported which deal with the existence and uniqueness of the solution to the inverse problems involving such systems [15–17].

The purpose of this paper is to develop a new method based on quasireversibility. It can be considered as an alternative to optimization based methods. In most optimization based methods, one seeks to minimize a cost functional which is a measure of the error. It leads to an iterative algorithm which often requires a large number of iterations for *satisfactory* convergence [18,19]. The present method assumes that the unknown function is *close* to a known background field. It is then possible to treat the linearized problem. The method uses the given data and, through an appropriate change of function [1,2,20], relates the inverse problem at hand to an overspecified boundary value problem (BVP) for an integro-differential parabolic equation. The present algorithm uses the method of quasireversibility [21] to solve the associated BVP, after which it can readily solve for the sought-after unknown coefficient. It also leads to an iterative algorithm, however, it requires a far fewer number of iterations for convergence than optimization based algorithms. We have considered one-dimensional [22] and two-dimensional [18] domains and, using optimization based algorithms, we needed at least 1800 iterations for satisfactory recovery. The present algorithm requires about 150 iterations.

In Section 2, we present the formulation and apply the method of quasireversibility to obtain the solution to the associated BVP. In Section 3, we use a number of numerical examples to discuss the algorithm in detail. In particular, we study applications from heat conductions as well as optical tomography, and Section 4 is devoted to closing remarks.

2. PROBLEM STATEMENT AND QUASIREVERSIBILITY

Consider a physical system for which the state $u(t,x)$ is governed by a parabolic equation given by

$$u_t = u_{xx} - a(x)u, \qquad t \in [0,\tau], \quad x \in [0,\ell], \tag{1}$$

with a Robin boundary condition at $x = 0$ and Neumann boundary condition at $x = \ell$,

$$u_x(t,0) + \alpha u(t,0) = 0, \qquad u_x(t,\ell) = f(t),$$

where constant $\alpha \geq 0$, and initial condition

$$u(0,x) = f_0(x),$$

where, $u(t,x)$ is the local temperature in heat conduction problems [23], and the light intensity in the case of optical tomography [24]. The boundary conditions at both ends can be altered according to the applications. The medium is excited by a specified flux at one boundary, i.e.,

$x = \ell$. If the light intensity at both boundaries, $u(t,0)$ and $u(t,\ell)$, in addition to the flux $u_x(t,0)$ are recorded, i.e.,

$$u(t,0) = y_1(t), \qquad u_x(t,0) = y_2(t), \qquad u(t,\ell) = y_3(t),$$

then the inverse problem for the above equation is to recover the absorption coefficient $a(x)$ based on the known applied flux and the measurements collected at the boundaries.

It is worthwhile to mention here uniqueness results for this inverse problem; we refer to Theorem 9.2.1 in [25] and Theorem 4.7 in [26] for additional details. These results are valid if functions $y_1(t)$ and $y_3(t)$ belong to the range of a Laplace-like transform. That is, there should exist certain functions s_j such that

$$y_j(t) = \frac{1}{\sqrt{\pi t}} \int_0^\infty \exp\left(-\frac{\tau^2}{4t}\right) s_j(\tau)\, d\tau, \qquad j = 1, 3.$$

In this case, the above inverse problem can be reduced to a similar problem for the hyperbolic equation $v_{\tau\tau} = v_{xx} - a(x)v$ via inversion of this transform (although the inversion procedure is unstable, but it is useful for the proof of a uniqueness result). The point here is that proofs of uniqueness results are more advanced for the hyperbolic inverse problems as compared with their parabolic counterparts. Thus, using uniqueness theorems for the hyperbolic case, one can prove uniqueness results for our target inverse problem in the following two cases:

(i) $f_0(x) \equiv 0$, and
(ii) $f_0(x) \neq 0$ on $[0,\ell]$.

Let $u_0(t,x)$ be the field due to an assumed value for the absorption coefficient $a_0(x)$, which is related to the actual absorption coefficient $a(x)$, by $a(x) = a_0(x) + h(x)$, where $h(x)$ is the unknown perturbation. So, $a_0(x)$ is our guess for the background function, and $h(x)$ is an unknown perturbation of the background. We will use linearization with respect to $h(x)$. Hence, we assume that $h(x)$ is much smaller than $a_0(x)$, i.e., $\|h\|_{L_2[0,\ell]} \ll \|a_0\|_{L_2[0,\ell]}$. Therefore, $u_0(t,x)$ is the solution of the equation

$$u_{0t} = u_{0xx} - a_0(x)u_0, \tag{2}$$

with the same boundary conditions as those for equation (1).

The equation for the error, i.e., $v(t,x) = u(t,x) - u_0(t,x)$, can be obtained by subtracting equation (2) from equation (1). This leads to

$$v_t = v_{xx} - a_0(x)v - h(x)u. \tag{3}$$

Linearization of equation (3) around u_0 leads to

$$v_t = v_{xx} - a_0(x)v - h(x)u_0. \tag{4}$$

The product $h(x)u_0$ suggests rewriting equation (4) in terms of a new function $H(t,x) = u/u_0 - 1$, which leads to

$$H_t = H_{xx} + 2H_x \frac{u_{0x}}{u_0} - h(x). \tag{5}$$

It is important that

$$H(x,0) = 0. \tag{5'}$$

Equation (5') is obviously true, if $f_0(x) \neq 0$ on $[0,\ell]$. In the case $f_0(x) = \delta(x - x_0)$, equation (5') was proven in [1] for the case of the Cauchy problem for the parabolic equation. However, it is rather difficult to prove equation (5') for other possible scenarios, if assuming, for example, that the domain for the variable x is bounded and $f_0(x) = \delta(x - x_0)$ or $f_0(x) \equiv 0$. Thus, similar to [2], we treat equation (5') as a conjecture in such cases. Equation (5) still has two unknowns, namely,

$H(t,x)$ and $h(x)$. However, $h(x)$ is not a function of time, and if we differentiate equation (5) with respect to time, then we obtain

$$P_t = P_{xx} + 2\frac{\partial}{\partial t}\left[\frac{u_{0x}}{u_0}\int_0^t P_x(\tau,x)\,d\tau\right], \qquad \text{where } P(t,x) = H_t(t,x). \tag{6}$$

This reduces the original inverse problem to an integro-differential equation with a Volterra-like integral for one unknown function, namely, $P(t,x)$. Once the solution for $P(t,x)$ is obtained, then the unknown perturbation $h(x)$ is found by integrating equation (5) from T_1 to T_2, i.e.,

$$h(x) = \frac{1}{T_1 - T_2}\int_{T_1}^{T_2}\left[H_t - H_{xx} - 2H_x\frac{u_{0x}}{u_0}\right]dt, \qquad \text{where } H(t,x) = \int_0^t P(\tau,x)\,d\tau. \tag{7}$$

The boundary conditions for the function P are provided by noting that the domain is accessible at both boundaries, therefore, the intensities and the fluxes are known. Once an initial absorption function is used, then the error in the intensities at the boundaries, i.e., $v(t,0)$, $v(t,\ell)$, and the error in the fluxes $v_x(t,0)$, $v_x(t,\ell)$ can be obtained. These in turn provide boundary conditions for the function $H(t,x)$,

$$H(t,0) = \frac{v(t,0)}{u_0(t,0)}, \qquad H_x(t,0) = \frac{v_x(t,0)u_0(t,0) - v(t,0)u_{0x}(t,0)}{u_0^2(t,0)}, \tag{8}$$

with similar relations for the boundary at $x = \ell$. Differentiating the boundary condition (8) with respect to time, we obtain the boundary conditions for the $P(t,x)$, according to

$$P(t,0) = H_t(t,0), \qquad P(t,\ell) = H_t(t,\ell), \qquad P_x(t,0) = H_{xt}(t,0), \qquad P_x(t,\ell) = H_{xt}(t,\ell). \tag{9}$$

Note that equation (6) for $P(t,x)$ is only of second order. However, we need to satisfy two boundary conditions on each side. Therefore, the boundary conditions are over-specified. Moreover, the initial condition $P(0,x)$ is unknown. Evaluating equation (5) at $t = 0$, we obtain

$$P(0,x) = H_t(0,x) = -h(x), \tag{10}$$

which is indeed the unknown function. Therefore, we are faced with solving an *ill-posed* problem (6), (8), and (9) for the function $P(t,x)$. Expanding equation (6) leads to

$$P_t = P_{xx} + 2P_x g + 2\dot{g}\int_0^t P_x\,dt, \qquad g(t,x) = \frac{u_{0x}}{u_0}. \tag{11}$$

This formulation was used in [1,2], where integrals were eliminated through truncated generalized Fourier series with respect to time (see the Introduction), and a Newton-like iterative process was used to deal with nonlinear dependence of the function $u(t,x)$ from the perturbation term $h(x)$. Now, however, we solve this problem without an elimination of the integral, which is similar to the idea of [20], where an inverse problem for a wave-like equation (with attenuation) in frequency domain was considered. So, to solve the BVP, we apply the method of *quasireversibility* [21]. Rewriting equation (11) in a compact form, we obtain

$$\mathcal{A}P = 2\dot{g}\int_0^t P_x\,dt, \qquad \text{where } \mathcal{A} = \frac{\partial}{\partial t} - \frac{\partial^2}{\partial x^2} - 2g\frac{\partial}{\partial x}. \tag{12}$$

In the method of quasireversibility, instead of solving equation (12) for $P(t,x)$, we solve

$$-\epsilon_2 P_{tt} + \mathcal{A}P + \frac{1}{\epsilon_1}\mathcal{A}^*\mathcal{A}P = 2\frac{1}{\epsilon_1}\mathcal{A}^*\dot{g}\int_0^t P_x\,dt, \tag{13}$$

where the operator $\mathcal{A}^*$ is formally adjoint to the operator $\mathcal{A}$, and small numbers ϵ_1 and ϵ_2 are regularization parameters. In the limit of $\epsilon_1, \epsilon_2 \to 0$, the solution to the above equation converges to the solution of the original equation in equation (11), at least in the case when the integral is not present in equation (11) [21]. The corresponding initial and final condition are given by [21]

$$P(0,x) - \epsilon_2 \frac{\partial P}{\partial t}(0,x) - \frac{1}{\epsilon_1}\mathcal{A}P(0,x) = P_0(x) - P_0^*(x), \qquad t = 0, \tag{14}$$

$$\epsilon_2 \frac{\partial P}{\partial t}(T,x) + \frac{1}{\epsilon_1}\mathcal{A}P(T,x) = 0, \qquad t = T, \tag{15}$$

where $P_0(x) = P(0,x)$ is the initial condition for $P(t,x)$, which is related to the unknown $h(x)$ in equation (10), thus unknown. The function $P_0^*(x)$ is any function in $L_2[0,\ell]$. According to [21], the choice of $P_0^*(x)$ will have influence on the solution $P(t,x)$ near the initial line $t = 0$ in a neighborhood of $O(\sqrt{\epsilon_2})$, for larger t, the effect of $P_0^*(x)$ will diminish as $\epsilon_1, \epsilon_2 \to 0$. Therefore, in the calculations for the first three examples, we choose $P_0^*(x) = P_0(x)$, so the right-hand side of equation (14) is homogeneous.

An alternative initial condition for equation (14) would be to use equation (10) instead, as is the case in Examples 4 and 5 below. Since we have no exact information on $h(x)$, initially, we can set $h(x) = 0$, then as an iterative inversion algorithm progresses, updated information on $h(x) = h^{\text{updated}}(x)$ can be used as the boundary condition

$$P(0,x) = -h^{\text{updated}}(x), \tag{14'}$$

where, initially, $h^{\text{updated}}(x) = 0$. We use equation (14′) in numerical Examples 4 and 5 below.

The term $\mathcal{A}^*\mathcal{A}$ leads to a fourth-order differential operator which enables us to enforce both boundary conditions on either side of the domain. Expanding equation (13), we obtain

$$-\hat{\epsilon}P_{tt} + \eta_1 P_t + \eta_2 P_x + \eta_3 P_{xx} + \eta_4 P_{tx} + P_{xxxx} = \eta_5 \int_0^t P_x\,dx + \eta_6 \int_0^t P_{xx}\,dx + \eta_7 \int_0^t P_{xxx}\,dx, \tag{16}$$

where $\hat{\epsilon} = (1 + \epsilon_1\epsilon_2)$ and

$$\begin{aligned}
&\eta_1 = \epsilon_1 + 2g_x, && g = \frac{u_{0x}}{u_0},\\
&\eta_2 = -2\epsilon_1 g + 4g_t - 8gg_x + 2g_{xx},\\
&\eta_3 = -\epsilon_1 + 2g_x - 4g^2, && \eta_4 = 4g,\\
&\eta_5 = -2g_{tt} - 2g_{txx} + 4g_x g_t + 4gg_{tx},\\
&\eta_6 = 4gg_t - 4g_{tx}, && \eta_7 = -2g_t.
\end{aligned}$$

Therefore, instead of solving equation (11) for $P(t,x)$, we are led to solve an elliptic boundary value problem depicted in Diagram A.

The solution of this problem gives an approximation to the function $P(t,x)$. This problem is well-posed and the solution is accurate everywhere except near a region close to the $t = 0$ and $t = T$ boundaries [21]. Now we have the following iterative inversion algorithms.

An Inversion Algorithm Based on Quasireversiblity

(1) Assume an initial absorption coefficient, $a_0(x)$, and solve for the field due to a_0 , i.e., $u_0(t,x)$.

(2) Use the given measurements and obtain boundary condition for $P(t,x)$, i.e., equations. (8),(9).

(3) Use the method of quasireversibility, i.e., equation (16), to solve for $P(t,x)$, and in turn, obtain $H(t,x)$ using $H(t,x) = \int_0^t P(\tau,x)\,d\tau$.

(4) Obtain the perturbation $h(x)$ using equation (7), and update according to $a_1(x) = a_0(x) + h(x)$.

(5) Repeat the process (1–4) until *satisfactory* convergence is achieved.

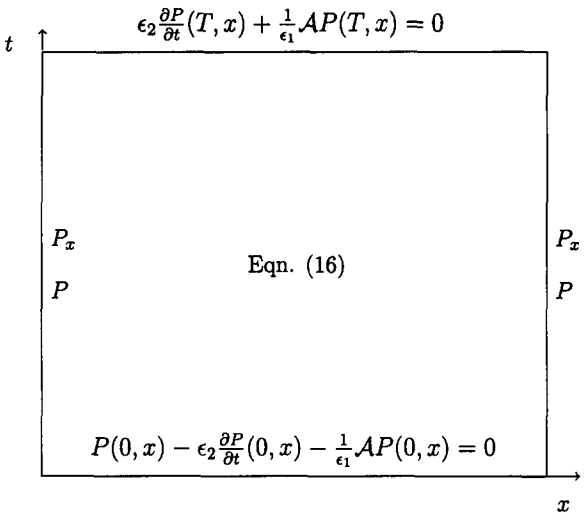

Diagram A.

In Step (4), we have to choose T_1, T_2 away from a boundary layer of thickness of at least $O(\sqrt{\epsilon_2})$ from both $t = 0$ and $t = T$ time lines. This is needed to avoid the influence of specific boundary condition (14) and (15) or (14'). At every iteration, the error can be computed and, as the iteration proceeds, it can be monitored for satisfactory reduction. It is our numerical experience that this iteration scheme converges. However, at this point, we cannot provide a rigorous proof of this fact. In the next section, we use a number of numerical examples to explain the algorithm in detail.

3. NUMERICAL IMPLEMENTATIONS AND EXAMPLES

For numerical implementation of the proposed inversion algorithm, high-order finite difference schemes for parabolic equations are used to discretize the partial differential equations [27]. The algorithm is composed of assuming an initial guess $a_0(x)$, for the absorption coefficient and then solving for the perturbation $h(x)$, which is then used to update the assumed guess according to $a_i(x) = a_{i-1}(x) + h(x)$. Once a background absorption function is assumed, then the field, $u_0(t,x)$, due to $a_0(x)$ is obtained. This involves the numerical integration of the parabolic equation given in equation (1). An implicit Crank-Nicolson time integration, together with a fourth-order finite difference spatial discretization leads to an accurate approximation. Once the background field $u_0(t,x)$ is known, then, using the given data, the error v at the boundaries can be obtained. With the known field $u_0(t,x)$ due to the assumed a_0, the function $g(t,x) = u_{0x}/u_0$ can also be computed. The discrepancies at the boundaries furnish the boundary conditions for the $P(t,x)$ according to equations (8),(9). For all the numerical results in this paper, the values of the parameters are given by $\epsilon_1 = \epsilon_2 = 10^{-5}$. There was little sensitivity to the values of these parameters. We obtained essentially the same results for $10^{-4} > \epsilon_1 = \epsilon_2 > 10^{-6}$.

Given the boundary conditions for the variable $P(t,x)$, the method of quasireversibility is used to find an approximation for the function $P(t,x)$ inside the domain. It is composed of solving the elliptic boundary value problem given in equation (16). Using at least a second-order accurate finite difference approximation for the terms in equation (16) leads us to the discretization given by

$$P_{tt} = \frac{1}{\Delta t^2}\left(P_i^{j+1} - 2P_i^j + P_i^{j-1}\right), \qquad P_t = \frac{1}{2\Delta t}\left(P_i^{j+1} - P_i^{j-1}\right), \tag{17}$$

$$P_x = \frac{1}{2\Delta x}\left(P_{i+1}^j - P_{i-1}^j\right),$$
$$P_{xxxx} = \frac{1}{\Delta x^4}\left(P_{i+2}^j - 4P_{i+1}^j + 6P_i^j - 4P_{i-1}^j + P_{i-2}^j\right), \tag{18}$$

$$P_{xx} = \frac{1}{3\Delta x^2} \times \left[t\left(P_{i-1}^{j+1} - 2P_i^{j+1} + P_{i+1}^{j+1}\right) + \left(P_{i-1}^j - 2P_i^j + P_{i+1}^j\right) + \left(P_{i-1}^{j-1} - 2P_i^{j-1} + P_{i+1}^{j-1}\right)\right], \tag{19}$$

$$P_{tx} = \frac{1}{4\Delta x \Delta t}\left(P_{i+1}^{j+1} - P_{i+1}^{j-1} - P_{i-1}^{j+1} + P_{i-1}^{j-1}\right), \tag{20}$$

where Δt and Δx are the step size in time and space. The approximation leads to a stencil of the form as shown in Diagram B.

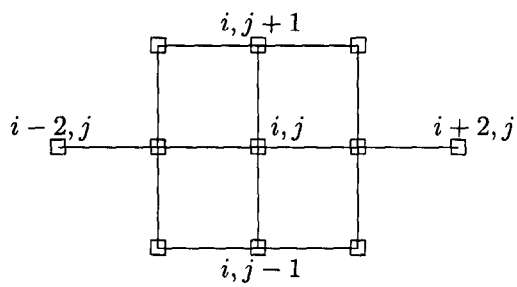

Diagram B.

The boundary conditions are imposed according to

$$P(j\Delta t, 0) = P_1^j, \qquad P_x(j\Delta t, 0) = \frac{1}{2\Delta x}\left(-3P_1^j + 4P_2^j - P_3^j\right),$$
$$P(j\Delta t, \ell) = P_{n+1}^j, \qquad P_x(j\Delta t, \ell) = \frac{1}{2\Delta x}\left(3P_{n+1}^j - 4P_n^j + P_{n-1}^j\right),$$

where n is the number of equal intervals in space. The initial condition in equation (14) simplifies to

$$\frac{\Delta t}{2\Delta x^2}P_{i-1}^2 - \left(1 + \epsilon_1\epsilon_2 + \frac{\Delta t}{\Delta x^2} + \frac{\epsilon_1 \Delta t}{2}\right)P_i^2 + \frac{\Delta t}{2\Delta x^2}P_{i+1}^2 + \frac{\Delta t}{2\Delta x^2}P_{i-1}^1 + \left(1 + \epsilon_1\epsilon_2 - \frac{\Delta t}{\Delta x^2} - \frac{\epsilon_1 \Delta t}{2}\right)P_i^1 + \frac{\Delta t}{2\Delta x^2}P_{i+1}^1 = 0.$$

Also, the condition at $t = T$ in equation (15) simplifies to

$$\left(\frac{\Delta t g_i^{m+1}}{2\Delta x} - \frac{\Delta t}{2\Delta x^2}\right)P_{i-1}^{m+1} + \left(1 + \epsilon_1\epsilon_2 + \frac{\Delta t}{\Delta x^2}\right)P_i^{m+1} + \left(-\frac{\Delta t g_i^{m+1}}{2\Delta x} - \frac{\Delta t}{2\Delta x^2}\right)P_{i+1}^{m+1} + \left(\frac{\Delta t g_i^{m+1}}{2\Delta x} - \frac{\Delta t}{2\Delta x^2}\right)P_{i-1}^m + \left(-1 - \epsilon_1\epsilon_2 + \frac{\Delta t}{\Delta x^2}\right)P_i^m + \left(-\frac{\Delta t g_i^{m+1}}{2\Delta x} - \frac{\Delta t}{2\Delta x^2}\right)P_{i+1}^m = 0,$$

where m is the number of time intervals. One way to solve the boundary value problem in equation (16) is to simply move all the terms to the left-hand side and invert a very big matrix. However, due to the integral terms on the right-hand side, the associated matrix would be a dense matrix and the inversion would be quite time consuming. An alternative approach would be to formulate an iterative algorithm in which the integral terms are kept on the right-hand side. In this case, the above discretization leads to a linear system of equations given by

$$\Gamma \mathbf{P}_{k+1} = \Lambda \mathbf{P}_k, \tag{21}$$

where the vector $\mathbf{P}_k$ contains the unknown function P_i^j at nodal points. The matrix Γ is the finite difference approximation of the terms on the left, and the matrix Λ is the finite difference approximation of the integral terms on the right. For this case, the matrix Γ is now a large but very sparse matrix, and special routines developed for sparse matrices can be used to effectively solve the associated linear system [28]. We use the routine DSLUGM from the SLATEC library. If the grid size in space and time are N_i and N_j, then the matrix Γ is of the size $(N_i \times N_j) \times (N_i \times N_j)$ and has $\approx 11(N_i \times N_j)$ nonzero entries. For the numerical examples in this paper, the iterations start from a zero initial guess $\mathbf{P}_0 = 0$, and we need no more than three iterations for convergence. Therefore, we have an outer iteration to update the $a(x)$ according to $a(x) = a_0(x) + h(x)$, and an inner iteration to solve for the $P(t, x)$.

EXAMPLE 1. Consider a one-dimensional heat conduction problem, in which there exists a temperature dependent heat generation. In this case, the conduction of heat is modelled by equation (1) with the unknown function $a(x)$ having a positive sign. This situation appears in a number of physical applications including the study of polymers [29], thermal analysis of superconductors [30], and biomedical heat generation [31]. For this case, the forward problem is given by the parabolic equation given by

$$\begin{gathered} u_t = u_{xx} + a(x)u, \qquad t \in [0, 0.6], \quad x \in [0, 1.0], \\ u_x(t, 1) = f(t), \qquad u(t, 0) = 0.1, \\ u(0, x) = 0.1. \end{gathered}$$

For the inverse problem, the measured data at the boundaries are provided according to

$$u_x(t, 0) = y_1(t), \qquad u(t, 1) = y_2(t).$$

Note that we have a nonzero initial condition and a Dirichlet type boundary condition at $x = 0$. The heat is added to the system through the flux boundary condition at $x = 1.0$ according to $f(t) = \exp(-(t - .2)^2/.005)$. Then, using the same numerical scheme, the flux at $x = 0$ and the temperature at $x = 1$ are calculated and are provided for the inversion.

The spatial domain is divided into 60 equal intervals and the time domain $[0, \tau]$ is divided into 150 equal intervals. At every iteration, the algorithm uses the given data and obtains boundary conditions for the P equation according to equations (8),(9). Figures 1 and 2 show the boundary conditions for the P equation for the first outer iteration, and Figure 3 shows the solution of the BVP in equation (16), i.e., $P(t, x)$, after three inner iterations. The solution is accurate everywhere, except for a narrow region close to the initial and final conditions.

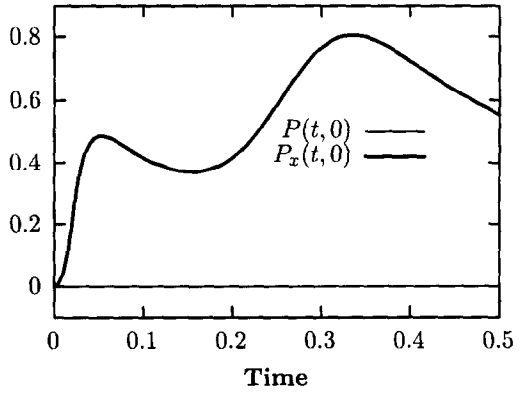

Figure 1. The boundary condition for the $P(t, x)$ at $x = 0$ for the first iterations in Example 1.

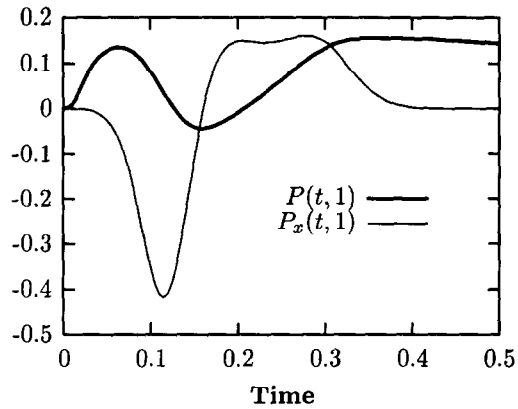

Figure 2. The boundary condition for the $P(t,x)$ at $x = \ell$ for the first iterations in Example 1.

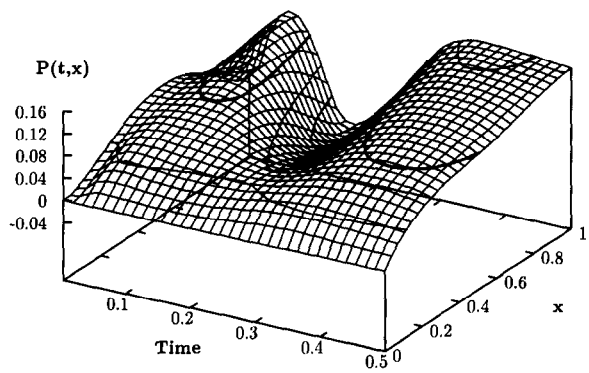

Figure 3. The solution of the BVP in equation (16) for $P(t,x)$ for the first outer iterations after three inner iterations for Example 1.

The algorithm then proceeds to compute the function $H(t,x)$ according to equation (7) after which it can solve for the perturbation $h(x)$, from equation (7). For this case, the interval $[T_1, T_2]$ is chosen as $[0.15, 0.25]$. In the first example, the function to be recovered is given by

$$\begin{aligned} a(x) &= 1, \qquad x \in [0, 0.48) \cup (0.62, 1], \\ a(x) &= 2, \qquad x \in [0.48, 0.62]. \end{aligned} \tag{22}$$

Figure 4 shows the convergence of the unknown function for the first 100 outer iterations. It also shows the actual function. Observe that the maximal value of the reconstructed function $a(x)$ is about 1.5, which is 75% of the target. The anomaly is located with good accuracy, although its image is 'diffusive', probably because of the diffusive character of the physical process. Figure 6 shows the reduction in the relative value of the error as a function of the number of iterations. The relative error is the total error divided by the error for the first iteration. The error for each iteration is given by

$$\text{Error} = \sum_{j}^{N} \left(y_1\left(j\Delta T\right) - u_x\left(j\Delta T, 0\right)\right)^2 + \sum_{j}^{N} \left(y_2\left(j\Delta T\right) - u\left(j\Delta T, \ell\right)\right)^2.$$

The quantity Error_0 is the above quantity for the first iteration.

EXAMPLE 2. In this example, we use the algorithm to recover a heat generation function given by

$$\begin{aligned} a(x) &= 1, \qquad x \in [0, 0.15) \cup (0.25, 0.75) \cup (0.85, 1], \\ a(x) &= 2, \qquad x \in [0.15, 0.25] \cup [0.75, 0.85]. \end{aligned} \tag{23}$$

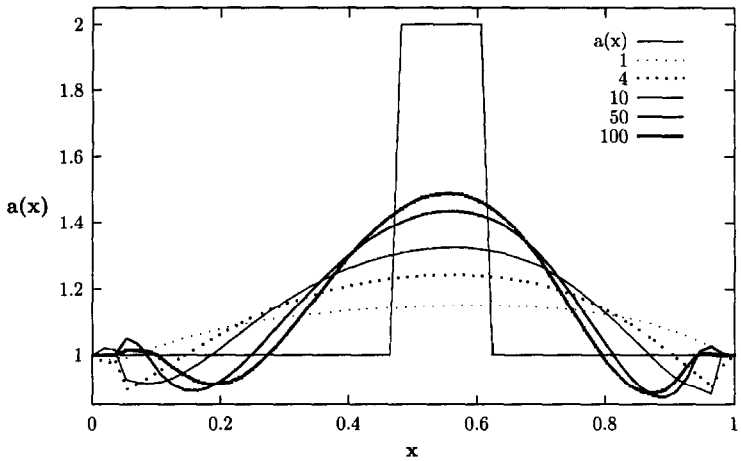

Figure 4. The convergence of the unknown heat generation function in Example 1.

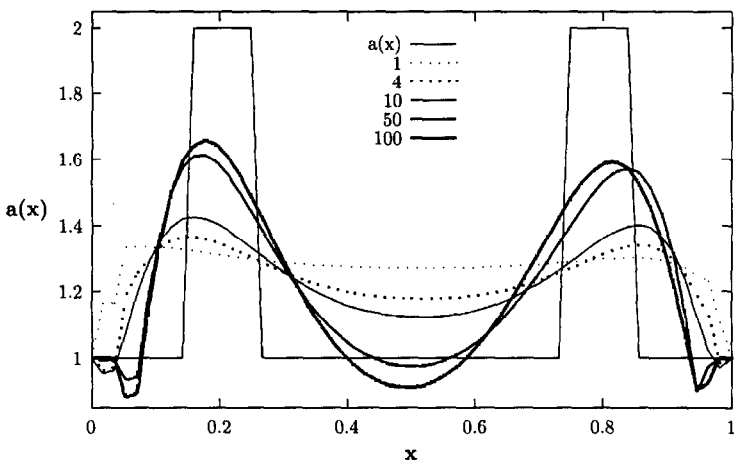

Figure 5. The convergence of the unknown heat generation function in Example 2.

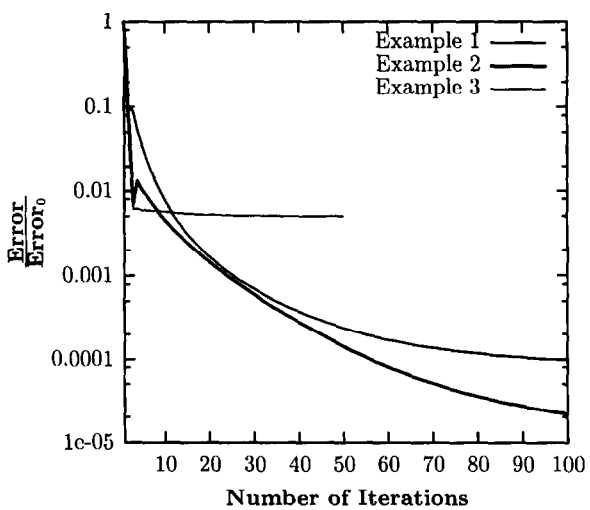

Figure 6. The reduction in the error computed at the boundaries for Examples 1–3 as a function of the number of iterations.

Figure 5 shows the convergence of the unknown function for a number of iterations. In both cases, the algorithm can recover a close approximation to the unknown function after a hundred iterations. The recovered function is more accurate if the anomaly is close to the boundaries where the data is being collected. In both cases, the results can also be improved by continuing the iterations. We next consider the effect of noise in the data.

EXAMPLE 3. Consider the problem of recovering the unknown function given in Example 2 and assume that the given data is noisy. For this problem, the measurements are the flux at $x = 0$ and the temperature at $x = 1$. Figure 7 shows the given data in which we have used a random number generator [32] to model the presence of noise. This was an additive noise with a zero mean with uniform distribution whose variance is equal to $\approx$ 5.E−5. Before using the given data, we use a three-point averaging approximation given by $f_i = (1/3)(f_{i-1} + f_i + f_{i+1})$, to somewhat smooth out the noise. Note that this is the crudest approach for filtering out the noise. Once the data is smoothed out, it can be readily differentiated by a finite-difference method to provide the necessary boundary conditions for the associated (BVP). Figure 8 shows the convergence of the unknown function for the noisy data. Compared to Figure 5, the result loses accuracy at the midpoint in the domain, but the algorithm can still recover a close estimate of the unknown function. Again, both locations of the target and the maximal values of the coefficient $a(x)$ within them are imaged with good accuracy. In particular, those maximal values differ from the correct ones by not more than 25%.

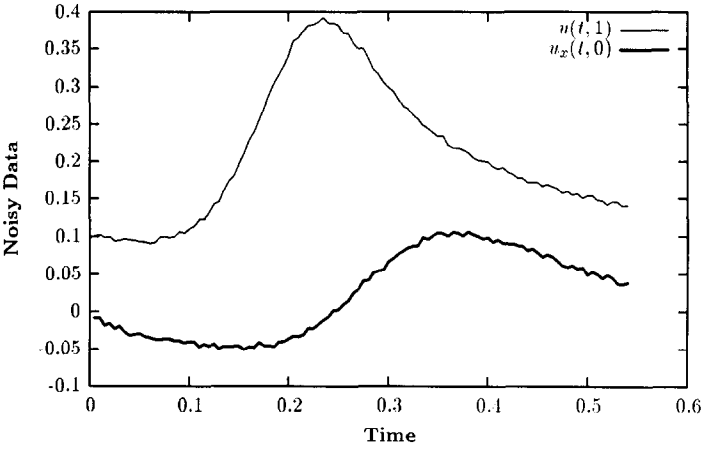

Figure 7. The collected data that are corrupted with noise in Example 3.

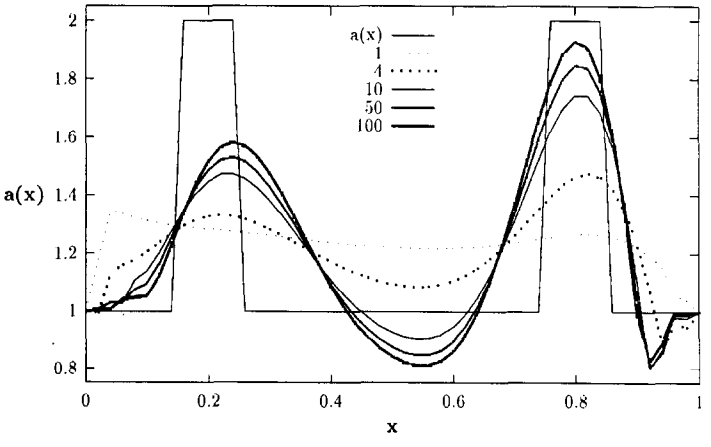

Figure 8. The convergence of the unknown heat generation function for the noisy data in Example 3.

Figure 6 shows the reduction of the error for the first three examples. The error is the difference between the given data at the boundaries and the calculated data from the system as the function $a(x)$ is updated after each iteration. For the case of noisy data, the error does not improve after 50 iterations. Figure 6 shows that the reduction in the error is not always monotonic. In optimization based methods, the algorithm seeks to minimize a cost functional which always includes the error. As a result, using such an algorithm [18], the error is reduced monotonically. However, in the present method, we deal directly with the given data. In the next two examples, noise is not introduced into the data.

EXAMPLE 4. We next consider a specific problem involving optical tomography with applications in medical imaging [1,6,7,21]. The mathematical model is given by equation (1):

$$u_t = Du_{xx} - a(x)u, \qquad t \in [0,\tau], \quad x \in [0,\ell],$$
$$u_x(t,\ell) = f(t), \qquad u_x(t,0) + \alpha u(t,0) = 0, \qquad u(0,x) = 0,$$

where D is the diffusion coefficient. For human tissues, these values are given by $D \approx 0.075(\text{mm}^2/\text{ps})$, $\alpha = 5(1/\text{mm})$, and $a \approx 0.0009(1/\text{ps})$ for healthy tissues, where ps stands for picosecond $= 10^{-12}$. If there exists an anomaly inside the domain, then the the absorption coefficient jumps to a value of about twice its normal amount, and the problem in medical imaging is to look for subsurface anomalies based on the data collected at the boundaries. The domain is excited by a specified flux $f(t)$ at $x = \ell$, i.e., $f(t) = \exp(-((t-1500)^2/300000))$, and the data are collected at both boundaries. For our purpose, the length $\ell = 5\,\text{cm}$ is appropriate. The time τ should be large enough for the excitation to reach the other end of the domain. We use $\tau = 15000\,\text{ps}$. In optical tomography, for the first $200 \sim 300\,\text{ps}$, there is not enough time for the excitation at $x = \ell$ to reach the boundary at $x = 0$, and the data for these initial times is corrupted. We use the value of zero for the first 300 ps. Note that, in this case, the sampling of the domain starts from a zero initial condition, i.e., $u(0,x) = 0$. As a result, applying the algorithm in its present form leads to numerical divergence at $t = 0$. The divergence occurs when evaluating the coefficient terms in equation (16). This is due to the presence of zero initial condition. As a result, we slightly modify the algorithm as follows.

At every outer iteration, we need to solve the equation for $P(t,x)$. This is done by inner iterations in which equation (21) is solved. For the special case of $u(0,x) = 0$, this iterative process fails to converge in a thin region close to $t = 0$. To overcome this divergence, we use the first iteration for $P(t,x)$ to generate the $H(t,x)$, and in turn, the perturbation $h(x)$. Note that the initial condition for $P(0,x)$ is indeed $P(0,x) = -h(x)$ from equation (10). Therefore, when performing the inner iterations, after the first inner iteration, we can use the boundary condition given in equation (14′), instead of the condition at $t = 0$ given in equation (14). This stabilizes the inner iterations and it converges after no more than three inner iterations.

We consider the recovering of an absorption coefficient given by

$$a(x) = 0.0009, \qquad x \in [0,0.7) \cup (1.2,3.7) \cup (4.2,5],$$
$$a(x) = 0.0018, \qquad x \in [0.7,1.2] \cup [3.7,4.2].$$

This function closely models the existence of two anomalies centered at 0.95 and 3.95. The spatial domain is again divided into 60 equal intervals and the time domain $[0,\tau]$ is divided into 150 equal intervals. We start the outer iterations by assuming an initial guess for the absorption coefficient $a_0(x) = 0.0009$. Figure 9 shows the recovering of the unknown function with two anomalies. The number of iterations needed for a satisfactory convergence is more than the heat conduction problems in Examples 1–3. The algorithm can recover a good estimate of the unknown function after ≈ 250 iterations. Figure 10 shows the reduction of the error as a function of the number of iterations.

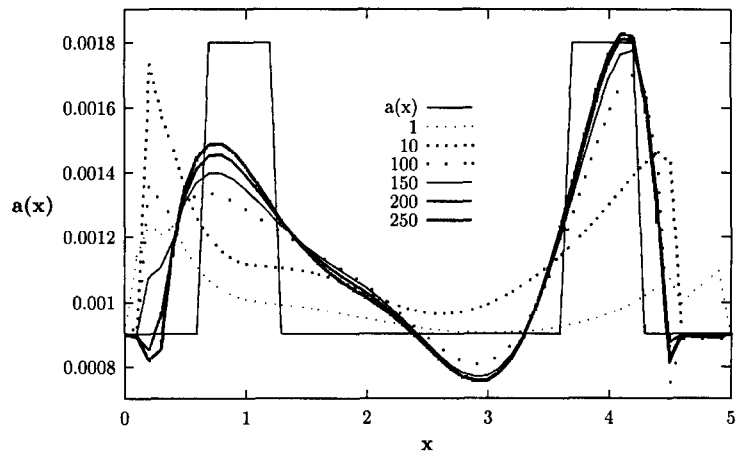

Figure 9. The convergence of the unknown absorption function in Example 4.

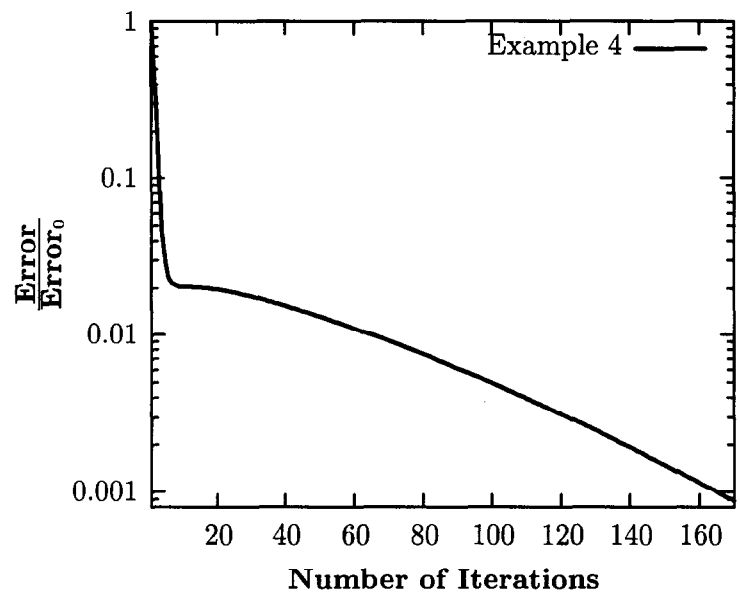

Figure 10. The reduction in the error computed at the boundaries for Example 4 as a function of the number of iterations.

4. DISCUSSION

The method uses the data collected at the boundaries and, in general, the results are more accurate if the anomaly is close to a boundary. This was also the case when we considered similar problems using an optimization based algorithm [18]. In this paper, we used a very crude method to smooth out the noise, and as a result, the presence of the noise affects the accuracy of the results and somewhat increases the number of iterations needed. However, the method can still recover a good estimate of the unknown functions. A similar observation of accurate imaging of both locations of the anomalies and the values of $h(x)$ within them was made in [20]. We note, however, that in previous works [1,2] on the ESM, only locations of the anomalies were imaged accurately, whereas values of the unknown coefficients within them were not calculated with good accuracy. Therefore, the second generation of the ESM, in which a BVP for an integro-differential equation is solved directly, rather than by an elimination of the integrals through truncated generalized Fourier series, has a clear advantage over the first generation of this method. Using the present algorithm, the computational time is considerably

lower. This is due to the fact that it requires a fewer number of iterations. We have considered one-dimensional [22] and two-dimensional [18] domains and, using optimization based algorithms, we needed at least 1800 iterations for satisfactory recovery. The present algorithm requires about 150 iterations. In addition, at every iteration, the present algorithm seeks the solution to a BVP which requires the inversion of a large but sparse matrix. The algorithm uses an efficient method specifically developed for sparse matrices.

In this paper, we presented a new method for one-dimensional parabolic inverse problems. The method requires temporal measurements obtained at the boundary. Since the method of quasireversibility [4] was developed for the solution of such problems for PDEs without integrals, our approach uses a modification of this method to solve that BVP, after which it can readily recover the unknown coefficient. The modification of the method of quasireversibility is done by the introduction of inner iterations for each outer iteration to deal with the integrals. Numerical results indicate that no more than three inner iterations are required for convergence at each iterative step of the outer iterations. Numerical results also indicate that an accurate estimate of the unknown coefficient can be recovered after about 150–200 outer iterations.

We considered two different applications with different initial and boundary conditions. For application in optical tomography, the algorithm is slightly modified to handle the divergence that can occur due to the physical constraints. Numerical results indicate that the algorithm can effectively recover the unknown function based on boundary measurements.

REFERENCES

1. M.V. Klibanov, T.R. Lucas and R.M. Frank, Fast and accurate imaging algorithm in optical/diffusion tomogrophy, *Inverse Problems* **13**, 1341–1361 (1997).
2. M.V. Klibanov and T.R. Lucas, Numerical solutions of a parabolic inverse problem in optical tomography using experimental data, *SIAM J. Appl. Math.* **59**, 1763–1789 (1999).
3. S.K. Bruke, Eddy-current inspection of cracks in a multilayer conductor, *Journal of Applied Physics* **67** (1), 465–76 (1990).
4. T.J. Martin and Dulikravich, Inverse determination of steady heat convection coefficient distribution, *Journal of Heat Transfer* **120**, 328–334 (1998).
5. K.J. Dowding, J.V. Beck and B.F. Blackwell, Estimating temperature-dependent thermal properties, *Journal of Thermophysics and Heat Transfer* **13** (3), 328–336 (1999).
6. R. Barbour, H. Graber, J. Chang, S. Barbour, S. Koo and R. Aronson, MRI guided optical tomography, *IEEE Comp. Sci. Engng.* **2** (4), 63–77 (1995).
7. National Research Council, *Mathematics and Physics of Emerging Biomedical Imaging*, National Academic Press, Washington, DC, (1996).
8. J. Taler, Analytical solution of the overdetermined inverse heat conduction problem with an application to monitoring thermal stresses, *Heat and Mass Transfer* **33**, 209–218 (1997).
9. C. Glorieux, J. Moulder, J. Basart and J. Thoen, The determination of electrical conductivity profiles using neural networks inversion of multi-frequency eddy-current data, *Journal of Physics D: Appl. Phys.* **32**, 612–622 (1999).
10. F. Berntsson, A spectral method for solving the sideways heat equation, *Inverse Problems* **15**, 891–906 (1999).
11. M.F. Martiz, G.T. Herman and C. Yee, Recovery of the absorption coefficient from diffused reflected light using a discrete diffusive model, *SIAM Journal on Applied Mathematics* **59**, 58–71 (1998).
12. P.L. Stoffa and M.K. Sen, Nonlinear multiparameter optimization using genetic algorithms: Inversion of plane-wave seismograms, *Geophysics* **56**, 1794–1810 (1991).
13. R. Keys, An application of Marquardt's procedure to the seismic inversion problem, *IEEE Proceeding* **74**, 476 (1986).
14. O. Pade and A. Mandelis, Computational thermal-wave slice tomography with back-propagation and transmission reconstructions, *Rev. Sci. Instrum.* **64**, 3548–3562 (1993).
15. I. Knowles, Uniqeness for an elliptic inverse problem, *SIAM Journal on Applied Mathematics* **59**, 1356–1370 (1999).
16. V. Isakov, Some inverse problems for the diffusion equation, *Inverse Problems* **15**, 3–10 (1999).
17. S. Gatti, An existence result for an inverse problem for a quisilinear parabolic equation, *Inverse Problems* **14**, 53–65 (1998).
18. M. Tadi, Evaluation of a two-dimensional conductivity function based on boundary measurements, *Journal of Heat Transfer* **217**, 367–372 (2000).
19. K.T. Nguyen and M. Prystay, An inverse method for estimation of the initial temperature profile and its evolution in polymer processing, *International Journal of Heat and Mass Transfer* **42**, 1969–1978 (1999).

20. Y.A. Gryazin, M.V. Klibanov and T.R. Lucas, Numerical solution of a subsurface imaging inverse problem, *SIAM J. Appl. Math.* (Submitted).
21. R. Lattes and J. Lions, *Method of Quasi-Reversibility: Applications to Partial Differential Equations*, Elsevier, New York, (1969).
22. M. Tadi, Inverse heat conduction based on boundary measurements, *Inverse Problems* **13**, 1585–1605 (1997).
23. H.S. Carslaw and J.C. Jaeger, *Conduction of Heat in Solids*, Oxford Science, New York, (1996).
24. B.B. Das, F. Liu and R.R. Alfano, Time resolved fluorescence and photon migration studies in biomedical and modern random media, *Rep. Progr. Phys.* **60**, 227–292 (1997).
25. V. Isakov, *Inverse Problems for Partial Differential Equations*, Springer-Verlag, New York, (1998).
26. M.V. Klivanov, Inverse problems and Carleman estimates, *Inverse Problems* **8**, 575–596 (1992).
27. J.C. Tannehill, D.A. Anderson and R.H. Pletcher, *Computational Fluid Mechanics and Heat Transfer*, Taylor and Francis, Washington, DC, (1997).
28. O. Axelsson, *Iterative Solution Methods*, Cambridge, New York, (1996).
29. B.R. Baliga, Thermal modeling of polymerizing polymethylmethacrylate, considering temperature-dependent heat generation, *Journal of Biomechanical Engng.* **114**, 251–259 (1992).
30. S.Y. Seol, Y.S. Cha and W.J. Minkowycz, Thermal analysis of composite superconductors subjected to time-dependent disturbances, *Heat and Mass Transfer* **33**, 177–184 (1997).
31. K.N. Rai and S.K. Rai, Heat transfer inside the tissues with a supplying vessel for the case when metabolic heat generation and blood perfusion are temperature dependent, *Heat and Mass Transfer* **35**, 345–350 (1999).
32. W. Press, W. Vetterling, S. Teukolsky and B. Flannery, *Numerical Recipes*, Cambridge, New York, (1992).